



# The Monthly Rates of TV Sporadic Meteors Between 2014 and 2021

Alberto S. Betzler<sup>1</sup>

Received: 3 October 2022 / Accepted: 31 March 2023 / Published online: 12 April 2023  
© The Author(s), under exclusive licence to Springer Nature B.V. 2023

## Abstract

This work presents a new method for estimating the population index of meteor showers using the entire distribution of meteors, thus avoiding the arbitrary choice of a threshold magnitude. This method was used to estimate the monthly population indices of 9771 sporadic meteors observed by the Brazilian Meteor Observation Network (BRAMON) between 2014 Aug. and 2021 Feb. The magnitude threshold was derived from the parameters of a Tsallis'  $q$ -exponential distribution proposed by Betzler & Borges (2015) and fitted to the observed distribution of apparent magnitudes. Population indices show temporal variation between May and September relative to the average monthly index ( $3.63 \pm 0.01$ ). The primary sources between May and September have a  $\lambda_{\odot}$  solar longitude associated with helion and antihelion sources. A secondary source has a time-varying solar longitudes and a larger number of meteors than the helion source between July and November. The secondary source has solar longitudes probably related to sporadic meteors in the north toroid. The helion and antihelion sources have average  $\lambda_{\odot} = 352$  and 215 degrees and radii of 8 and 4 degrees, respectively.

**Keywords** Methods: observational · Methods: statistical · Meteorites · Meteors · Meteoroids

## 1 Introduction

The cumulative distribution of meteor magnitudes  $m$  is usually modeled by an exponential function (Baggaley 1977) as

$$N_{\leq}(m) = Cr^m, \quad (1)$$

---

✉ Alberto S. Betzler  
betzler@ufrb.edu.br

<sup>1</sup> Centro de Ciência e Tecnologia em Energia e Sustentabilidade, Universidade Federal do Recôncavo da Bahia, Feira de Santana, Bahia 44085-132, Brazil

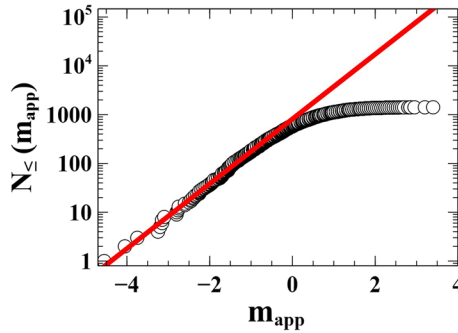


**Fig. 1** Inverse cumulative distribution  $N_{\leq}(m_{app})$  of the number of sporadic meteors observed by BRAMON in each August from 2014 to 2020 as a function of their apparent visual magnitude  $m_{app}$ . The circles represent the observed meteors and the solid red line is the fit of the Eq. (1) with  $C = 814 \pm 7$  and  $r = 4.61 \pm 0.03$  and for meteors with  $m_{app} \leq -0.7$ . August is a month with a particularly high number of faint meteors in all BRAMON data. The apparent magnitude threshold is defined using the arguments presented in Sect. 3.3

where  $N_{\leq}(m)$  is the cumulative flux<sup>1</sup> of meteors brighter than magnitude  $m$ ,  $C$  is a constant, and  $r$  is the population index defined as the ratio of total meteors observed with magnitude  $m$  to those with magnitude  $m + 1$ . The  $r$  index allows the determination of the meteoroid mass flux and their size distribution or the prediction of a meteor shower. Vaubaillon et al. (2005).

The population index is obtained by fitting the Eq. (1) to the observed meteor magnitude distribution (Fig. 1). However, this equation fits only the brightest events, not the entire observed distribution.

There are numerous examples, especially in strongly interacting systems, where the fit to exponential or exponential-like distributions is limited to a narrow range of the spectrum. In some of these cases, the incomplete fit may be due to observational errors caused by instrumental limitations leading to finiteness effects or by data collection or analysis methods. However, there are also cases where the incomplete fit is not due to observations but to a physical cause.

Population indices of the same meteor shower estimated using an exponential law such as Eq. (1) usually show considerable differences. These differences are due to the search for a suitable magnitude threshold, as shown by the multiplicity of population indices of sporadic meteors in table 4 of Ohsawa et al. (2020).

It is also important to define the range of magnitude variation for the definition of  $r$  using the Eq. (1). However, this information is sparse in most studies analyzing this parameter.

In this work, it is proposed to use a generalization of Eq. (1) that incorporates the exponential distribution into the threshold for bright meteors and also naturally tends to an upper bound for higher brightness values of magnitudes, as observed in the data so that the threshold can be estimated using the entire data set and not just an arbitrary portion of it.

<sup>1</sup> The representation of the cumulative distribution most commonly used in statistical contexts for a random variable  $M$  where  $M$  takes a value less than or equal to  $m$  is  $N(M \leq m)$ . The more compact notation  $N_{\leq}(m) \equiv N(M \leq m)$  is chosen to avoid the capital character  $M$ , since this symbol has a different meaning in this work, namely the mass of a meteoroid.

This generalized distribution is a  $q$ -exponential distribution previously used by Betzler and Borges (2015) for meteor shower analysis. The magnitude threshold derived from the fitted parameters of the  $q$ -exponential distribution on observational data was used to determine the monthly population indices of sporadic meteors observed in double or multiple stations of the Brazilian Meteor Observation Network (BRAMON).

The sources of sporadic meteors from BRAMON were associated with the temporal variations of these population indices.

## 2 The Data

BRAMON is one of the largest meteor observing networks in the Southern Hemisphere, in terms of number of stations (130) and area covered ( $1.3 \times 10^6$  km). Most BRAMON stations are located in south-central Brazil, where the largest urban centers are São Paulo and Rio de Janeiro, with the remaining stations located in the northeast and west of the country. The geographic arrangement of the stations allows detection of meteors in a declination range between  $-90$  and  $+70$  degrees. The stations are equipped with a TV camera that can record astrometric and photometric data of meteors, allowing the study of their dynamic and physical properties.

A typical BRAMON station is equipped with a Samsung SCB 2000 camera, which uses a Sony Super HAD 1/3 CCD sensor and can register light sources with intensities as low as 0.05 lux. These cameras were modified with the removal of the infrared filter (IR) and combined with a Varifocal Ai 3–8 mm Dc F1.0 Ltvr-3 lens. This lens provided a field of view (FOV) of  $\sim 70 \times 60$  degrees for the shortest focal length.

The BRAMON uses the UFOCapture<sup>2</sup> software to detect meteors. The UFOCapture software works in conjunction with UFOAnalyzer and UFOORBIT, making it more suitable for meteor surveys. UFOANALYSER classifies the detected objects (meteors, aircraft, insects, etc.) in the videos. Each class is defined based on configurable parameters such as brightness, pixel size, geometry and duration. The SKYMAP star catalog (Myers et al. 1997) is overlaid on an image extracted from the recorded video to determine the meteor radiant in the sky (ecliptic latitude and longitude) and the apparent magnitude of the object over time, which can allow the creation of light curves.

BRAMON recorded 9,771 sporadic meteors at double or multiple stations between August 2014 and February 2021. The apparent magnitudes of these meteors were separated by month to create monthly magnitude distributions, and related to the ecliptic longitude of their radiants.

## 3 Theoretical Approach

The distribution of apparent magnitudes of meteors can be modeled using a  $q$ -exponential distribution, as proposed by Sotolongo-Costa et al. (2008) and reformulated by Betzler and Borges (2015), summarized in the following.

The relative probability  $P_{\geq}(M)$  for the inverse cumulative number of meteoroids  $N_{\geq}(M)$  with mass equal to or greater than  $M$  is given by

<sup>2</sup> [http://sonotaco.com/soft/e\\_index.html](http://sonotaco.com/soft/e_index.html).

$$P_{\geq}(M) = \frac{N_{\geq}(M)}{N_T} = \int_M^{\infty} p(M') dM', \tag{2}$$

with  $N_T$  the total number of meteors,

and  $p(M')$  the probability density of meteoroids with mass  $M'$  within an error  $dM'$ .  $p(M')$  is considered a  $q$ -exponential distribution (see details in Betzler and Borges (2015)), so the cumulative distribution becomes

$$N_{\geq}(M) = N_T(1 + bM)^{\frac{2-q}{1-q}}, \tag{3}$$

which can be rewritten as

$$N_{\geq}(M) = N_T [\exp_q(-\beta M)]^{2-q}, \tag{4}$$

with  $b = (q - 1)\beta$ . The  $q$ -exponential that appears in Eq. (4) (Tsallis 1994) is defined by  $\exp_q(x) = [1 + (1 - q)x]^{1/(1-q)}$  if  $[1 + (1 - q)x] > 0$  and  $\exp_q \equiv 0$  otherwise. The  $q$ -exponential presents two important features: i) it recovers the exponential function as  $q \rightarrow 1$  ( $\lim_{x \rightarrow 1} \exp_q(x) = \exp(x)$ ); ii) it exhibits a power-law behavior,  $\exp_q(-x) \approx x^{1/(1-q)}$  for  $x \gg 1$  and  $q > 1$ , so, **for large mass meteoroids**,

$$N(M) \sim M^{-n}, \tag{5}$$

with  $n = (2 - q)/(q - 1)$ . Magnitude  $m$  and mass  $M$  are considered to be exponentially correlated ( Sotolongo-Costa et al. 2008, ):

$$M = M_0 e^{-\gamma m}, \tag{6}$$

with  $M_0 = M(m = 0)$  and  $\gamma$  is the magnitude/mass conversion parameter.

The Eq. 6 is a reasonable approximation considering that the meteors of a meteor shower have a small scatter in terms of altitude, geocentric velocity, and zenith distance (Moorhead et al. 2021), parameters that can be used to define the mass of the meteoroid by an exponential equation (Jacchia et al. 1965). This approach also applies to sporadic meteors in each month, since they originate from certain celestial regions as anthelion and helion sources.

Since  $M = M(m)$  is a monotonically decreasing function, the substitution of Eq. (6) into the inverse cumulative distribution of the mass of meteors (Eq. 4, number of meteors with mass higher than or equal to  $M$ ) leads to the cumulative distribution of the magnitudes of meteors ( $N_{\leq}(m)$ , the number of meteors with magnitudes less then or equal to  $m$ ):

$$N_{\leq}(m) = N_T [\exp_q(-\beta_m e^{-\gamma m})]^{2-q}, \tag{7}$$

where  $\beta_m = \beta M_0$ . The  $\beta_m$  constant is a fitting parameter in the procedure. A power of a  $q$ -exponential can be rewritten as another  $q$ -exponential with a different index  $q'$

$$N_{\leq}(m) = N_T \exp_{q'}(-\beta'_m e^{-\gamma m}), \tag{8}$$

with  $\frac{1}{1-q'} = \frac{2-q}{q-1}$  and  $\beta'_m = (2 - q)\beta_m$ . Graphical representation of Eq. (8) in logarithm scale (log with base 10) and the abscissa (magnitude) in linear scale is shown in Fig. 2. For bright objects, this equation displays an ascending straight line with slope  $a$  given by:

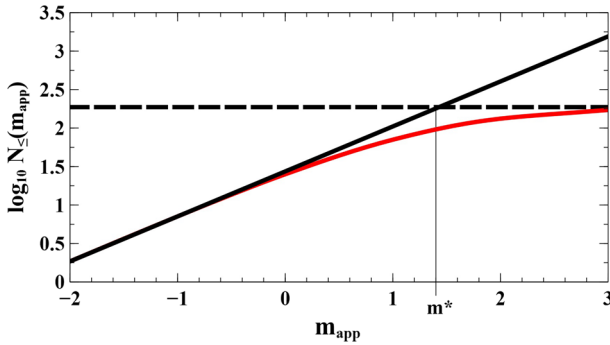


**Fig. 2** Graphical representation of the Eq. (8) for  $N_T = 193.2$ ,  $q' = 1.95$ ,  $\beta'_m = 6.23$ , and  $\gamma = 1.31$ . These parameters correspond to the best fit of this equation to the distribution of apparent magnitudes of the Eta Aquarids meteor shower observed by BRAMON in 2015. The solid black line is the Eq. (1), which is the asymptotic limit of Eq. (8) for bright meteors. The slope of the solid black line is  $\gamma \log_{10} e / (q' - 1)$ . The dashed black line is  $\log_{10} N_T$ , the asymptotic limit of Eq. (8). The intersection of the solid black line and the dashed black line gives the transition magnitude, in this case  $m^* = 1.4$

$$a = \frac{\gamma \log_{10} e}{q' - 1}, \tag{9}$$

corresponding to the rare event’s region. This same region is covered by Eq. (1), with a slope equal to  $\log_{10} r^*$ .

The cumulative distribution tends to its upper value  $N_T$ , and the semi-logarithmic plot shows a horizontal asymptote for high values of the magnitudes. The transition magnitude  $m^*$  between the extension of the ascending straight line of the region of the rare event and the horizontal line of the horizontal asymptote is given by

$$m^* = \frac{1}{\gamma} \ln [(q' - 1)\beta'_m]. \tag{10}$$

### 3.1 Meteor Limit Magnitude × Transition Magnitude

Kingery and Blaauw (2017) listed the possible sources for the limit magnitude of a system: camera hardware and software, sky conditions, and the angular velocity of the meteors. The limit magnitude of the meteors  $m_L$  could be 1-3 magnitudes brighter than the stellar limit magnitudes  $m_s$ , taking these factors into account. Moreover, this limit magnitude can change significantly during the night, even between cameras at the same station. The limit magnitude for meteor detection is given by

$$m_L = m_s - 2.5 \log_{10}(d) \tag{11}$$

with

$$d = \frac{180 \cdot r_e \cdot V_g \cdot \tau \cdot \sin \zeta}{\pi \cdot \text{FOV} \cdot R \cdot \text{FWHM}}, \tag{12}$$

where  $r_e$  is the horizontal camera resolution,  $\tau$  is the integration time, FWHM is the full width at half maximum of the images, measured at the unsaturated stars,  $V_g$  is the velocity

of the meteor,  $\zeta$  is the angle between the camera pointing direction and the radiant, and  $R$  is the range to the meteor.

The BRAMON stations are equipped with similar cameras. Thus, considering a meteor from the same dynamical group,  $d$  is inversely proportional to  $R$ . Meteors with a larger trajectory in the FOV tend to be better detected than those with short duration and/or low angular velocity. There is an abundance of sources for the meteors observed by BRAMON. Meteors with the same  $R$  and different dynamical and geometrical parameters ( $V_g$  and  $\zeta$ ) may or may not be registered by the same camera.

The apparent magnitude of the faintest meteor detected at each BRAMON station was used to estimate the observed meteor limit magnitude  $m_L$ . The Shapiro-Wilk test suggests that the distribution of meteor limit magnitudes from the stations follows a Gaussian curve with a confidence level greater than 0.10, with an average network limit magnitude  $3 \pm 1$  ( $1 \sigma$ ). This statistical analysis allowed me to establish a meteor limit magnitude equal to 3 for BRAMON.

The transition magnitude  $m^*$  (Eq. 10) does not have the same value as the meteor limit magnitude  $m_L$ . The transition magnitude  $m$  is normally distributed, with a mean of  $0.3 \pm 0.2$  magnitudes (Table 1), and it is different from the BRAMON meteor limit magnitude ( $m_L = 3$ ).

The parameters of the Eq. 8 were estimated from the monthly magnitude distributions to obtain the transition magnitudes  $m^*$ .

### 3.2 Parameter Estimation

The parameters of the Eqs. (1) and (8) were found by optimization using the nonlinear generalized reduced gradient for line search and the Pearson chi-squared coefficient as the objective function. The mean values  $q' = 2.3$ ,  $\gamma = 1.1$ , and  $\beta'_m = 2$  from Betzler and Borges (2015) were adopted as initial estimates for the optimization of Eq. (8). The initial estimate for the parameter  $N_T$  was obtained directly from the amount of meteors in the monthly BRAMON magnitude distributions.

### 3.3 Definition of the Population Indexes

It is not recommended to use the same value as a threshold magnitude for applying the Eq. (1) for different meteor showers, even if the same detector is used. An arbitrary magnitude does not necessarily guarantee that this exponential function is asymptotic to the observed distribution.

An alternative way to define the  $r$  indices is to set a threshold for the magnitude based on the properties of the distribution or a particular parameter describing the meteor shower. Pokorný and Brown (2016) has defined this threshold using Bayesian statistical methods.

The monthly population index  $r$  was defined in this work using the magnitude threshold  $m^* - 1$ . The index  $r$  tends asymptotically to  $r$  when the magnitude threshold  $\ll m^*$ . However,  $r$  corresponds to very bright meteors and makes comparison with the published population index for sporadic meteors difficult. This magnitude threshold provides an  $r$  index from fitting the Eq. 1 to the observed magnitude distribution with a coefficient of determination greater than 0.95.

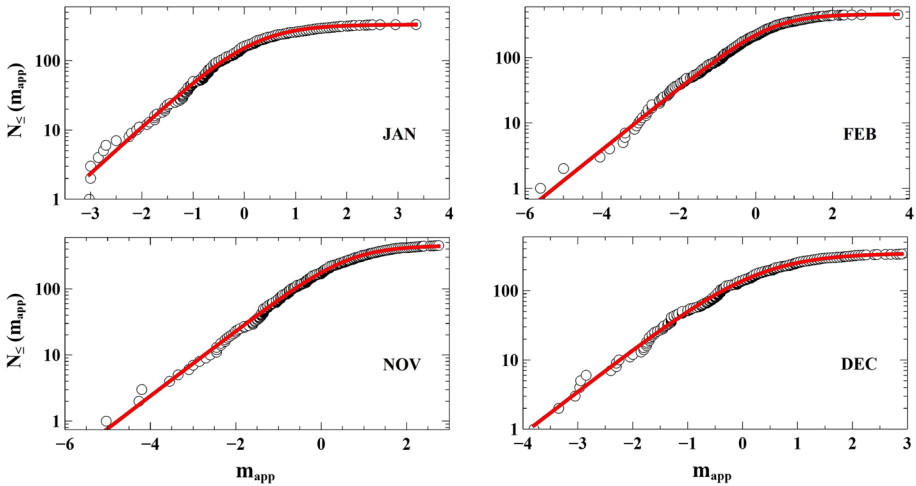
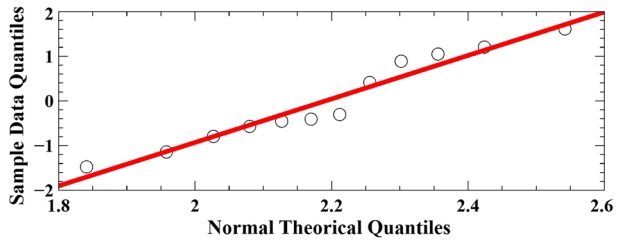


**Fig. 3** Observed cumulative distribution  $N_{\leq}(m_{app})$  of sporadic meteors detected by BRAMON in four months from 2014 to 2021 (circles). The solid red curves correspond to the best fits obtained with Eq. (8)

**Fig. 4** Quantile-quantile diagram derived from the distribution of the monthly index  $q'$  of the sporadic meteors (sample data) and their normal distribution (theoretical normal distribution)



## 4 Analysis and Results

### 4.1 The Average Value and Meaning of the Index $q'$

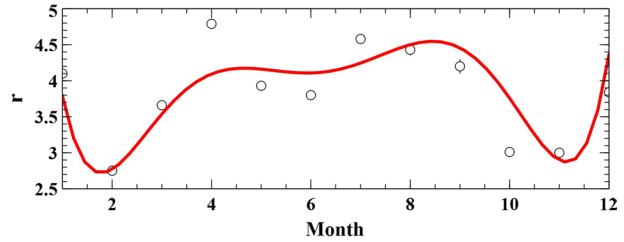
The chi-squared scores suggest that a  $p$ -value  $\sim 1$  was obtained by fitting of the Eq. (8) to the observed monthly cumulative distribution of the sporadic meteors obtained between 2014 and 2021 (Fig. 3).

These  $p$ -values suggest that Eq. (8) is suitable for modeling the apparent magnitudes obtained with BRAMON TV cameras and visual and photographic data, as shown by Betzler and Borges (2015) and Borges and Betzler (2020).

The index  $q'$  of the Eq. (8) can be adequately approximated by a normal distribution, given a confidence level greater than 0.05 (Fig. 4). The average value of the entropic index is  $q' = 2.2 \pm 0.2$ , and agrees with  $q' = 2.0 \pm 0.1$  estimated by fitting the magnitude distributions of selected meteor showers in the Visual Meteor Database (VMDB) (see Betzler and Borges 2015, ).

One possible interpretation for obtaining similar values for  $q'$  from different data is that the sporadic meteors and the meteor showers may have the same formation process, regardless of how they were obtained. This process may have a physical origin or the effect of an observational bias or both. A value of  $q' \neq 1$  indicates that other effects besides short-range

**Fig. 5** Evolution of the population index  $r$  along one year. The solid red line corresponds to a 6th degree polynomial fitted empirically to the data (Table 1)



forces can affect these distributions if only a physical origin of the observed distribution is considered.

## 4.2 Monthly Population Indices

The monthly population indices of the sporadic meteors are in the Table 1. The indices show a temporal variation (Fig. 5). In the optical domain, this time dependence was also noted by Rendtel (2004) in his VMDB database analysis and by Vida et al. (2020) using Electron-multiplying CCDs meteor data.

The Spearman correlation coefficient  $R_s$  was calculated to examine the relationship between the population indices and the number of meteors. This test indicates that the relationship between the two variables cannot be considered statistically significant ( $R_s = 0.57$ ). The temporal variations in the data cannot be caused by environmental factors, even though most BRAMON stations are located under tropical climates, with average annual precipitation ( $\sim 1000$  mm) and a dry season between May and August.

There are two definite sources of sporadic meteors of variable strength in time and heliocentric longitude in the monthly population indices. The indices have their minima in February and November, and become relatively constant (a plateau) between May and September. Absolute maxima are in January and December, when the proportion of faint meteors is more frequent than the average population index. The weighted arithmetic mean of the monthly BRAMON indices is  $r = 3.63 \pm 0.01$ , similar to the visually estimated index  $3.73 \pm 0.01$  obtained by Hughes (1974) between 1947 and 1956 using a  $-5 \leq m_{app} \leq 0$  magnitude range, in Canada. The population index of sporadic meteors determined by Vida et al. (2020) is  $2.55 \pm 0.06$ , which is lower than our value and  $r = 2.95 \pm 0.06$  determined by Rendtel (2004). The value of Vida et al. (2020) was attributed to bad weather in some months of the year that affected meteor detection, but a comparison between the population indices  $r$  and  $r^*$  of the table (1) suggests that the difference between the measures may be due to the use of a different threshold magnitude. These authors used a threshold magnitude of 2.2, which is different from the mean of the BRAMON transition magnitude ( $m^* = 0.3$  magnitudes). In Rendtel (2004) there is no information about the threshold magnitude, but it is probably similar to the value used by Vida et al. (2020). However, this last hypothesis should be taken with caution: Betzler (2022) pointed out that the population index  $r$  is likely to be affected by the difference in detection probability between visual and TV observing methods, as well as by the zenith distance of the radiant of the meteor shower, even assuming a similar threshold magnitude for their definition.

The main source of the plateau and the maxima in January and December have solar longitudes that are probably associated with the helion and antihelion sources found in



**Fig. 6** Histograms of the distributions of  $\lambda_{\odot}$  solar longitudes of sporadic meteors with  $m_{app} \leq m^* - 1$  (table 1) obtained by BRAMON between May and July from 2014 to 2021. The August distribution was created using data from 2014 to 2020

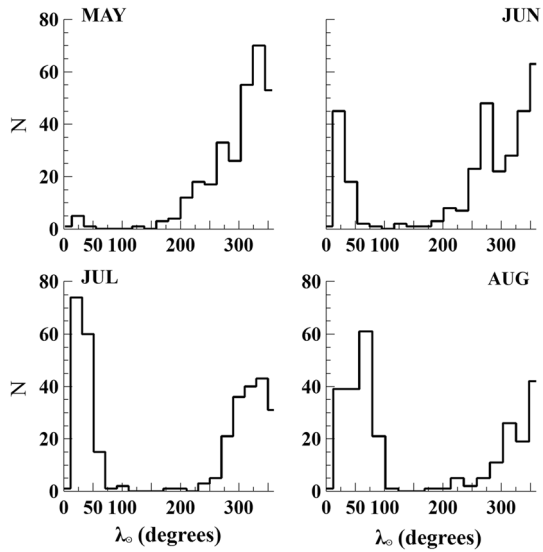


**Table 1** Monthly population indices and meteor sources of sporadic meteors during a year.  $r^* = 10^a$  is the population index calculated with the slope  $a$  from Eq. 9.  $m^*$  is the magnitude threshold (Eq. 10)

Month	$r^*$	$m^*$	$r$	$N_T$	S1	N1	S2	N2
1	4.71	0.19	$4.1 \pm 0.2$	332	218.8	25	x	x
2	2.96	0.41	$2.75 \pm 0.02$	451	236.6	37	x	x
3	3.94	0.08	$3.66 \pm 0.06$	528	270.4	37	x	x
4	5.26	0.01	$4.79 \pm 0.07$	940	294.3	47	x	x
5	4.05	0.43	$3.93 \pm 0.04$	1269	334.5	70	24.0	5
6	3.95	0.40	$3.80 \pm 0.04$	1362	359.9	63	21.3	45
7	4.75	0.19	$4.58 \pm 0.04$	1813	339.9	43	21.3	74
8	6.94	0.34	$4.61 \pm 0.03$	1415	358.9	42	67.8	61
9	4.69	-0.05	$4.2 \pm 0.1$	547	359.3	17	77.6	34
10	3.10	0.61	$3.01 \pm 0.05$	326	357.8	9	122.4	43
11	3.10	0.63	$3.00 \pm 0.02$	451	353.1	5	129.0	33
12	4.10	0.26	$3.84 \pm 0.09$	337	211.5	28	x	x

$r$  is the population index for  $m_{app} \leq m^* - 1$ .  $N_T$  is the total number of meteors. S1 and S2 (degrees) are the solar longitudes of the meteor source. N1 and N2 are the number of meteors in the S1 and S2 solar longitude bins

radar meteor surveys (Jones and Brown 1993; Galligan and Baggaley 2005). The helion source has a mean solar longitude  $\lambda_{\odot} = 352$  deg. and a radius of 8 degrees, based on plateau, October, and November data.

The antihelion source has a mean solar longitude  $\lambda_{\odot} = 215$  deg. and a radius of 4 degrees based on January and December data (Fig. 6 and Table 1). Transitions to antihelion-apex and apex-helion sources occur in February and April. The population indices in the plateau have secondary sources with a temporally variable number of meteors and solar longitude, which are larger than the the helion source between July and November, and do not correspond to the radiant of major meteor showers such as the Eta Aquarids

and Perseids ( $\lambda_{\odot} \approx 45.5$  and  $=140$  deg, respectively, (Hajduk and Buhagiar 1982; Arlt 2003)). The secondary source has solar longitudes probably related to the north toroidal sporadic meteor source (Campbell-Brown and Wiegert 2009). The apex is the main meteor source in March.

## 5 Conclusions

In this work, a new method for estimating the population index is proposed that uses the entire distribution of meteors, thus avoiding the arbitrary choice of the threshold magnitude. As an example of the application of the method, the monthly population index was estimated using BRAMON data for sporadic meteors from 2014 to 2021, and the following results were obtained:

1. The inverse cumulative monthly distribution of apparent magnitudes of sporadic meteors recorded by TV cameras is well modeled by a  $q$ -exponential distribution proposed by Betzler and Borges (2015).
2. The average value of the entropic index is  $q' = 2.2 \pm 0.2$  and is consistent with  $q' = 2.0 \pm 0.1$  estimated by fitting the visual magnitude distributions of meteor showers in the VMDB. This  $q'$  index suggests the same formation process for the analyzed magnitude distribution of sporadic meteors and meteor showers, regardless of the observational method used.
3. The monthly population indices of sporadic meteors show a temporal variation. The indices have their minimum in February and November and a plateau between May and September. Absolute maxima are in January and December, when the proportion of faint meteors is more frequent than the mean population index (weighted arithmetic mean  $r = 3.63 \pm 0.01$ ).
4. The main source of the plateau and the maxima in January and December have solar longitudes probably associated with the helion and antihelion sources, respectively. The apex is the most important meteor source in March.
5. The antihelion source has a mean solar longitude  $\lambda_{\odot} = 215$  degrees and a radius of 4 degrees, based on January and December data.
6. The helion source has a mean solar longitude  $\lambda_{\odot} = 352$  degrees and a radius of 8 degrees based on plateau, October and November data.
7. The population indices in the plateau have secondary sources with a time-varying number of meteors and solar longitude, which are greater than the helion source between July and November. The secondary source has solar longitudes probably associated with the north toroidal sporadic meteor source.

**Acknowledgements** The author thanks all BRAMON citizen scientists who contributed to this research with data collection and processing, C. A. di Pietro and M. Zurita for kindly providing the BRAMON data, Ernesto P. Borges for his comments and suggestions in the preparation of this manuscript, and two anonymous reviewers for their constructive comments and recommendations, which definitely helped to improve the quality of the article.

**Data Availability** Some of the raw data on which this article is based are available in the EDMOND database (<https://tinyurl.com/y8oed5h7>). The processed data are available from A.S.B. on request.

## References

- R. Arlt, Radiant ephemeris for the Perseid meteor shower. WGN, J. Int. Meteor Organiz. **31**(1), 19–28 (2003)
- W.J. Baggaley, The mass distribution of large meteoroids. MNRAS **180**, 89–93 (1977)
- A.S. Betzler, A comparison of TV and visual derived population indexes of some meteor showers. eMeteor-News **7**(2), 106–108 (2022)
- A.S. Betzler, E.P. Borges, Non-extensive statistical analysis of meteor showers and lunar flashes. MNRAS **447**(1), 765–771 (2015)
- E.P. Borges, A.S. Betzler, Non-Boltzmannian distributions observed in small bodies of the Solar System. Rendiconti dell'Accademia Nazionale delle Scienze detta dei XL - Memorie e Rendiconti di Chimica **44**, 89–97 (2020)
- M. Campbell-Brown, P. Wiegert, Seasonal variations in the north toroidal sporadic meteor source. M & PS **44**(12), 1837–1848 (2009)
- D.P. Galligan, W.J. Baggaley, The radiant distribution of AMOR radar meteors. MNRAS **359**(2), 551–560 (2005)
- A. Hajduk, M. Buhagiar, Southern and Northern Hemisphere Observations of the Eta Aquarid Meteor Shower in 1969–1978. Bull. Astron. Instit. Czechoslovakia **33**, 262 (1982)
- D.W. Hughes, The influx of visual sporadic meteors. MNRAS **166**, 339–344 (1974)
- L.G. Jacchia, F. Verniani, R.E. Briggs, A Analysis of the Atmospheric Trajectories of 413 Precisely Reduced Photographic Meteors. *SAO Special Report*, 175 (1965)
- J. Jones, P. Brown, Sporadic meteor radiant distributions - Orbital survey results. MNRAS **265**, 524 (1993)
- A. Kingery, R.C. Blaauw, Determination of the meteor limiting magnitude. P & SS **143**, 67–70 (2017)
- J.R. Myers, C.B. Sande, A.C. Miller, W.H. Warren, J. D.A. Tracewell, VizieR Online Data Catalog: SKY2000 - Master Star Catalog (Myers+ 1997). *VizieR Online Data Catalog*, p. V/95 (1997)
- A.V. Moorhead, T. Clements, D. Vida, Meteor shower radiant dispersions in global meteor network data. Monthly Notices Royal Astron. Soci. **508**(1), 326–339 (2021)
- R. Ohsawa, A. Hirota, K. Morita, S. Abe, D. Kastinen, J. Kero, C. Szasz, Y. Fujiwara, T. Nakamura, K. Nishimura, S. Sako, J.-I. Watanabe, T. Aoki, N. Arima, K. Arimatsu, M. Doi, M. Ichiki, S. Ikeda, Y. Ita, T. Kasuga, N. Kobayashi, M. Kokubo, M. Konishi, H. Maehara, T. Miyata, Y. Mori, M. Morii, T. Morokuma, K. Motohara, Y. Nakada, S.-I. Okumura, Y. Sarugaku, M. Sato, T. Shigeyama, T. Soyano, H. Takahashi, M. Tanaka, K. Tarusawa, N. Tominaga, S. Urakawa, F. Usui, T. Yamashita, M. Yoshikawa, Relationship between radar cross section and optical magnitude based on radar and optical simultaneous observations of faint meteors. P & SS **194**, 105011 (2020)
- P. Pokorný, P.G. Brown, A reproducible method to determine the meteoroid mass index. A & A **592**, A150 (2016)
- J. Rendtel, *The population index of sporadic meteors*, pp. 114–122 (2004)
- O. Sotolongo-Costa, R. Gamez, F. Luzón, A. Posadas, P. Weigandt & Beckmann, Non extensivity in meteor showers. *Apeiron: Studies in Infinite Nature*, 15 (2008)
- C. Tsallis, What are the numbers that experiments provide. Quimica Nova **17**(6), 468–471 (1994)
- J. Vaubaillon, F. Colas, L. Jorda, A new method to predict meteor showers. I. Description of the model. A & A **439**(2), 751–760 (2005)
- D. Vida, M. Campbell-Brown, P.G. Brown, A. Egal, M.J. Mazur, A new method for measuring the meteor mass index: application to the 2018 Draconid meteor shower outburst. A & A **635**, A153 (2020)

**Publisher's Note** Springer Nature remains neutral with regard to jurisdictional claims in published maps and institutional affiliations.

Springer Nature or its licensor (e.g. a society or other partner) holds exclusive rights to this article under a publishing agreement with the author(s) or other rightsholder(s); author self-archiving of the accepted manuscript version of this article is solely governed by the terms of such publishing agreement and applicable law.